Measurement of $\pi^+ d \rightarrow \Delta^{++} n$ at intermediate energy

P. V. Pancella,* G. S. Mutchler, S. D. Baker, J. W. Kruk, I. M. Duck, M. D. Corcoran, G. C. Phillips, J. M. Clement, and J. A. Buchanan
T. W. Bonner Nuclear Laboratories, Physics Department, Rice University, Houston, Texas 77251

B. W. Mayes and L. S. Pinsky
University of Houston, Houston, Texas 77004

W. von Witsch
Universität Bonn, Federal Republic of Germany

Eduardo Andrade
Universidad Nacional Autonoma de México, Circuito Exterior C.U., México 20, Distrito Federal, Mexico

H. Garcilazo†
Kernforschungszentrum Karlsruhe, Universität Karlsruhe, Federal Republic of Germany

J. M. Laget
Centre d'Etudes Nucleaires de Saclay, Gif-sur-Yvette, France
(Received 24 August 1987)

The threefold differential cross sections for the reaction $\pi^+ d \rightarrow \Delta^{++} n \rightarrow \pi^+ pn$ were measured in a kinematically complete experiment as a function of beam momentum and the $\Delta(1232)$ production angle. The cross sections were measured at seven beam momenta between 312 and 600 MeV/c for $\theta_\Delta = 55°$ and 91° in the center-of-mass system. Angular distributions from 30° to 119° (c.m.) were taken at beam momenta of 350 and 425 MeV/c. These data are compared with predictions from a unitary, relativistic, three-body theory based on the Faddeev equations and with a multiple scattering theory. The theories reproduce the general trend of the data except at the highest energies.

I. INTRODUCTION

Pion-induced deuteron breakup is one of the principal testing grounds for models of three-body dynamics with nuclear forces. In the energy region below 1 GeV there is considerable evidence that the relevant degrees of freedom are nucleons, Δ's, and pions interacting predominantly in S and P waves.[1] Current models describe the three-body breakup reaction in terms of the various two-body interactions between the beam pion and the two constituent nucleons of the deuteron. These models do not explicitly take into account the $N\Delta$ interactions. These are interesting not only because the Δ dominates the pion-nucleon interaction in this energy range, but also because dibaryon resonances, if they exist, have small elasticity and hence their partial width is significantly larger for the three-body channel ($B^2 \rightarrow N\Delta \rightarrow \pi pn$), than for the two-body channels ($B^2 \rightarrow pp$ and $B^2 \rightarrow \pi d$). This has been demonstrated in Faddeev calculations, by Araki *et al.*[2] in multiple scattering calculations, by Duck and Umland,[3] and in model calculations by Grein *et al.*[4] A primary goal of the present experiment is to study the three-body breakup reaction in regions of phase space far from the dominant quasifree scattering peak. By the appropriate choice of kinematics, we have measured the angle and energy dependence of a $\pi d \rightarrow \Delta^{++} n$ cross section for the first time, at beam kinetic energies between 200 and 475 MeV. In so doing, we have also extended the kinematic range of previous $\pi^+ d \rightarrow \pi^+ pn$ differential cross-section measurements.

A. Choice of kinematics

In an attempt to isolate the $n\Delta$ final state interaction, the kinematics of the $\pi^+ d \rightarrow \pi^+ pn$ reaction were chosen to emphasize events in which the invariant mass of the final state pion-proton subgroup is near the peak of the Δ^{++} mass. At the same time, other well-known scattering processes such as quasifree scattering [QFS, Fig. 1(a)] were suppressed. Since the strong dependence of the QFS cross section on the spectator nucleon momentum makes the effect of a nucleon-delta interaction difficult to observe, the spectator nucleon was required to have at least 100 MeV/c of momentum in the laboratory frame. In addition, the πn subgroup mass was required to be less than 1150 MeV/c^2, to suppress interference from the Δ^+ resonance. This choice of kinematics also has the effect of suppressing final state interactions (FSI) between the two nucleons [Fig. 1(c)] because of their large relative momentum.

Data were taken at the 24 angle and energy combinations listed in Table I. The angles are defined in Fig. 2. $\theta_{\rm dec}$ in Table I is the angle between the proton trajectory

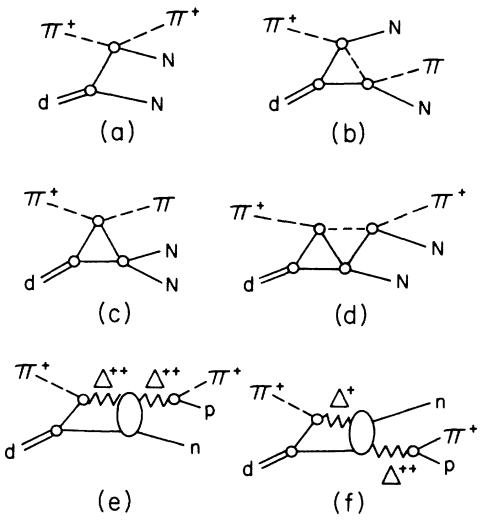

FIG. 1. Feynman diagrams for $\pi^+ d \to \pi^+ pn$. (a) Quasifree scattering; (b) with πN final state interaction; (c) with NN final state interaction. (d) Pion double scattering with NN final state interaction. (e) ΔN interaction, direct. (f) ΔN interaction, exchange.

and the Δ particle's c.m. velocity vector, measured in the rest frame of the Δ. The threefold differential cross sections were measured at seven beam momenta from 312 to 600 MeV/c at $\theta_{\Delta \text{c.m.}} = 55°$ and 91° and at several angles between 30° and 120° for 350 and 425 MeV/c beam momenta.

B. Previous studies of $\pi^+ d \to \pi^+ pn$

The qualitative aspects of the reaction $\pi^+ d \to \pi^+ pn$ are well described by a simple impulse approximation

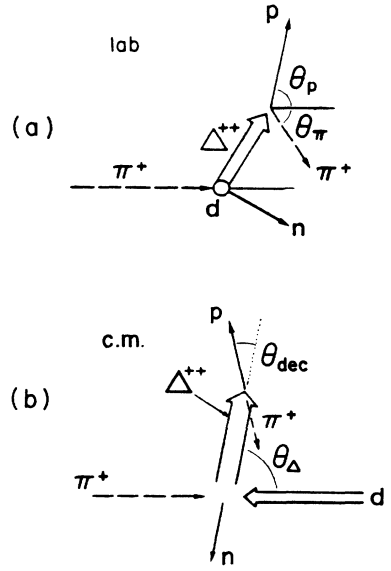

FIG. 2. $\pi^+ d \to \pi^+ pn$ kinematics. Δ^{++} production and decay, (a) in the lab frame, and (b) in the reaction center of mass frame.

(SIA). In this model, the pion interacts with one of the nucleons in the loosely bound deuteron and the other nucleon is a spectator. The SIA is expected to be a good approximation in regions of phase space where the spectator emerges with a laboratory momentum comparable to the deuteron Fermi momentum of less than 50 MeV/c. The SIA cross section is given by

$$\frac{d^3\sigma}{d\Omega_\pi d\Omega_p dP_\pi} = \frac{P_\pi^2 P_p^2 |M_{\text{SIA}}|^2}{128\pi^5 P_b E_\pi |E_n P_p^2 - E_p P_n \cdot P_p|} , \quad (1)$$

$$|M_{\text{SIA}}|^2 = \Phi_d^2(P_n) \left[16\pi^2 S_{\pi N} \left[\frac{d\sigma}{d\Omega} \right]_{\pi N \to \pi N} \right] , \quad (2)$$

where the quantities in the square brackets are evaluated in the πN c.m. system, and Φ_d^2 is the deuteron wave function in momentum space. P_b is the beam pion laboratory momentum, and E_i and P_i are the total energy and three momentum of the reaction products in the laboratory frame. Thus the magnitude of the SIA cross section is determined by the deuteron wave function and the free π-nucleon cross section. This model predicts the correct qualitative features of the data, but gives absolute cross sections which are high by as much as a factor of 2 at the QFS peak and an order of magnitude elsewhere.

The first kinematically complete measurement of pion-induced deuteron breakup was by Bayukov *et al.*[5,6] with 1 GeV/c negative pions for spectator neutron momenta up to 200 MeV/c. The pions from the CD_2 target were detected in the angular range $\theta_\pi = 17°-23°$ by a magnetic spectrometer and the recoiling protons by a range spark chamber at $\theta_p = 70°$. Good agreement between the data and the SIA was obtained in the region of small momentum transfer to the spectator neutron, (≤ 80 MeV/c). At larger momentum transfers, good agreement was obtained by including the πN FSI and pn FSI [Figs. 1(b) and 1(c)]. At this relatively high beam energy, they found that the various diagrams are well separated in phase space.

Dakhno *et al.*[7-11] studied the reaction $\pi^- d \to \pi^- pn$ with a deuterium bubble chamber at pion momenta of 371, 438, and 552 MeV/c. They compared the data to an impulse approximation calculation by Obrant,[12] which included a coherent sum of pion single [Fig. 1(a)] and double scattering [Fig. 1(b)] amplitudes with a contribution from NN FSI [Fig. 1(c)]. Due to limited statistics the data are given as single, or in some cases doubly, rather than triply differential cross sections. Within the limitations imposed by this integration over angles, they conclude that at these lower energies, the contributions of the various diagrams overlap considerably and the interference leads to significant effects. For example, the pion rescattering reduces the QFS cross section by as much as 25%.

In a previous kinematically complete measurement by this group, the reaction $\pi^\pm d \to \pi^\pm pn$ was studied at 340 MeV/c with a liquid deuterium target (Hoftiezer *et al.*[13,14]). Data were obtained at 11 angle pairs, spanning a range of neutron momentum from 0 to 350 MeV/c. The protons were detected using a magnetic spectrometer and the pions using a time-of-flight (TOF)

arm. The shape of the differential cross section as a function of the proton momentum was reproduced by a coherent sum of the SIA, πN FSI, and NN FSI [Figs. 1(a), 1(b), and 1(c)], but the magnitude was larger than the data by as much as a factor of 2 at the QFS peak. The addition of pion rescattering in the entrance channel (DWIA) gave a good fit to the data for neutron momentum less than 40 MeV/c. For neutron momenta above 40 MeV/c the data were fit by adding a $J^{\pi}=2^{+}$ dibaryon, but at the cost of two adjustable parameters. Makarov *et al.*[15] were able to substantially improve the fit to the data using the Obrant formalism without the addition of the $^1D_2$ dibaryon.

Relativistic Faddeev calculations of the π d breakup reaction at the kinematics of Hoftiezer *et al.* have been published by Matsuyama[16] and by Garcilazo.[17] Both calculations use experimental data on πN and NN reactions as input, obey three-body unitarity constraints, and treat all particles relativistically. The principal differences are in the specific approximations and the treatment of the P_{11} partial wave in the πN system. Neither explicitly includes a direct interaction between the Δ and a nucleon. Matsuyama found that for small spectator momentum, the impulse contribution is dominant and determines the gross structure of the cross sections. He also found that higher-order processes such as πN FSI, NN FSI, and πd

TABLE I. $\pi^+ d \rightarrow \pi^+ pn$ angle pairs. The first column shows average beam momentum (energy) at the center of the target. $\Delta p/p$ was 1% except for 543 MeV/c (1.5%) and 597 MeV/c (2%). (All errors FWHM.) The second column is the corresponding total energy in the reaction center of mass. θ_π corresponds to the central lab angle of the spectrometer, θ_p the same for the TOF arm. The average acceptance for each arm about this central value appears at the bottom of the column. The minimum spectator momentum (neutron momentum) is given in the fifth column. The last two columns give the corresponding Δ production and decay angles, calculated for a Δ mass of 1232 MeV/c^2. The angles are defined in Fig. 2, $\theta_{\rm dec}$ is measured in the Δ rest frame relative to its c.m. velocity vector. The accepted range in $\theta_{\Delta\rm c.m.}$ is determined by the cuts shown in Fig. 8, the range in $\theta_{\rm dec}$ is approximate. The laboratory angles for the QFS scattering data are also listed in the third and fourth columns.

Beam momentum in MeV/c (kinetic) energy MeV)	$\sqrt{s}$ (GeV)	Lab. angles θ_π	Lab. angles θ_p	$P_n^{\rm min}$ (MeV/c)	$\Delta_{\rm c.m.}$ angles $\theta_{\Delta\rm c.m.}$	$\Delta_{\rm c.m.}$ angles $\theta_{\rm dec}$
311.6	2.195	80°	55°	87	55°	30°
(201.9)		55°	80°	117	91°	21°
		103°	30°		a	
		95°	35°	17	31°	34°
350.3		86°	45°	57	45°	30°
	2.225	75°	53°	68	55°	31°
(237.5)		65°	67°	111	75°	24°
		50°	75°	88	83°	30°
		37°	105°	140	119°	14°
		98°	31°		a	
387.6	2.255	75°	50°	58	55°	28°
(272.4)		42°	82°	95	91°	29°
		93°	30°	19	29°	32°
		80°	42°	28	45°	30°
425.0		70°	50°	46	55°	30°
	2.284	65°	55°	60	63°	28°
(307.8)		58°	65°	94	77°	23°
		50°	77°	138	91°	20°
		38°	91°	183	105°	20°
		30°	105°	221	119°	17°
		96°	31°		a	
483.8	2.329	60°	50°	75	55°	36°
(363.9)		35°	80°	250	91°	31°
		94°	31°		a	
543.0	2.375	60°	48°	140	55°	33°
(421.0)		33°	76°	325	91°	29°
		94°	30°		a	
597.0	2.417	58°	46°	193	55°	31°
(473.5)		30°	75°	395	89°	32°
		92°	30°		a	
Average acceptance		±2°	±5°		±5°	±10°

[a]QFS data.

multiple scattering in the initial channel increase the cross section, unlike the results quoted in Ref. 14. This was attributed to the inclusion of off-shell propagation of the πd system, while Ref. 14 only considered on-shell propagation. The calculation reproduces the data within a factor of 2–3 in the region of small spectator momentum. In regions of large spectator momentum, he found that the *NN* FSI increases the cross section by a factor of 2–5 and substantially improves the agreement over the impulse approximation. The Garcilazo calculation finds that higher-order terms reduce the impulse approximation in the region of small spectator momentum, and consequently gets substantially better agreement especially in the region of phase space where the mass of the $\pi^+ p$ subsystem is near the Δ^{++} mass. In both calculations there are severe discrepancies between the theory and the data below 400 MeV/c proton momentum at some angle pairs.

Goetz *et al.*[18] measured the $\pi^- d \rightarrow \pi^- pn$ reaction at 150 MeV/c using a CD_2 target. The pions were detected with a spectrometer at 77.5° and 90° and the neutrons (protons) at 40°±9.5° with a large area neutron (proton) detector. The data are presented as double differential cross sections and compared with the SIA. The data, not unexpectedly, show significant discrepancies from this simple model. One unusual feature is the fact that the data are higher than the SIA at the QFS peak unlike the results quoted above. They also give the ratio of the neutron to proton cross sections, which are somewhat above the ratio predicted by the SIA (~9:1). Hoftiezer *et al.*[13] calculate this ratio, by comparing their π^+ and π^- data. They find that the ratio is about 9:1 near the QFS peak and reduces to 1:1 for large spectator momenta. With a nucleon angular acceptance of 19°, the data of Goetz *et al.* represent neither a point in phase space nor a 4π solid angle. Thus a detailed comparison with a more elaborate calculation is largely lost due to the integration of the cross sections over the neutron angles.

Finally, Gyles *et al.*[19] have measured the $\pi^+ d \rightarrow \pi^+ pn$ differential cross section and vector analyzing power at 340 and 410 MeV/c using a CD_2 target. Both the pion and the proton were detected by TOF in six detectors each. This gives kinematically complete data at 36 angle pairs at 340 MeV/c and 56 angle pairs at 410 MeV/c and represents the most detailed breakup data set to date. At the five angle pairs in common with the data of Hoftiezer *et al.*, they find good agreement above a proton momentum of 400 MeV/c, but their data are significantly smaller below this momentum. The cause of this discrepancy is not known, but may stem from the energy-loss corrections of either data set, or the solid angle corrections of the data of Hoftiezer *et al.* Gyles *et al.* observe the dominance of the pole diagram at small spectator momentum, the dominance of the *pn* FSI at low proton momentum, and no significant enhancements in the region of the Δ^{++} mass. They compare their data to the Faddeev calculations of Garcilazo *et al.*[17,20,21] and conclude that this theory reproduces the data quite well without any exotic effects such as dibaryons. The same group, List *et al.*,[22] took additional data at 410 MeV/c at nine angle pairs chosen to emphasize the *np* final state interactions. They compare to a new version of the Garcilazo theory,[23] which allows off-mass shell propagation. This improves the agreement in the *np* FSI region, but has little effect in the QFS region.

II. THE EXPERIMENT

A. Apparatus

This experiment used positive pions from the LAMPF P^3 beam channel at seven different momenta. The momentum spread of the beam ranged from 1% at 312 MeV/c to 2% at 597 MeV/c. The apparatus is shown schematically in Fig. 3. Two pivoting arms viewed a liquid deuterium target in the shape of an upright cylinder, 7.62 cm high and 5.72 cm in diameter. The target was contained in a thin-walled (0.025 cm) Kapton flask within a vacuum chamber. The areal density of the target was 2.81×10^{23} deuterons per cm^2, averaged over the beam cross section.

The scattering angles of outgoing charged particles in each arm were measured with multiwire proportional chambers (MWPC's P1–P6). In addition, a magnetic spectrometer measured the momentum of the final state pions with a resolution $\Delta p/p = 1.5\%$ full width at half maximum (FWHM). With time-of-flight measurements to provide particle identification, this makes for a kinematically complete experiment. Scintillation counters (S1–S4) measured times of flight and provided fast coincidence signals which triggered the MWPC's. Only pions were counted in the spectrometer, and were required to be in coincidence with protons in the other arm. The FWHM angular acceptance of the system was $\Delta\theta_\pi = \pm 2°$, $\Delta\phi_\pi = \pm 2.2°/\sin(\theta_\pi)$ in the spectrometer, and $\Delta\theta_p = \pm 5°$, $\Delta\phi_p = \pm 2.5°/\sin(\theta_p)$ in the straight arm.

The original design of this spectrometer [Argonne Large Acceptance Spectrometer (LAS)] is described by Colton.[24] We operated the LAS with the following differences: The MWPC's after the magnet were replaced (P5 and P6) with slightly smaller, operationally identical detectors, the bend angle was reduced from 45° to 30°, the quadrupole doublet in the LAS was not energized, and vacuum was maintained in the quadrupole beam pipe; particles traveled through air in the rest of the arm.

These changes increased the allowed particle momentum, reduced the accepted solid angle to about 10 msr, and made the tracking of particles much more straightforward and reliable. The bend angle was vertical, decoupling the momentum-dependent acceptance from the scattering angle measurement.

B. Calibration

Two integrating wire chambers were employed to monitor the beam profile and position before and after the target (PM1 and PM2). These were the principal diagnostics for beam tuning. Two independent scintillator telescopes (M1-M6) viewed the target at 30° above and below the beam axis as relative monitors of the beam intensity multiplied by the target density. (See elevation inset, Fig. 3.) The apparatus was calibrated at each setting of the beam using two different reference reactions. First,

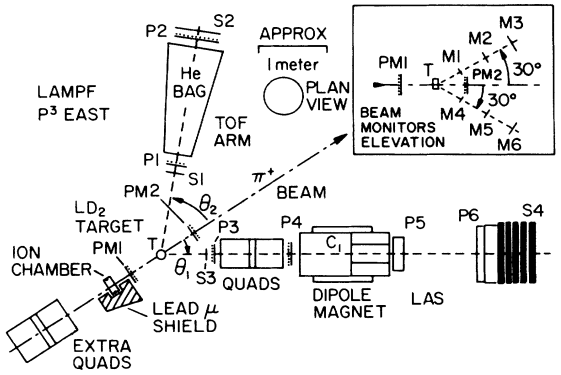

FIG. 3. Apparatus. Schematic plan view and beam monitors' elevation (inset).

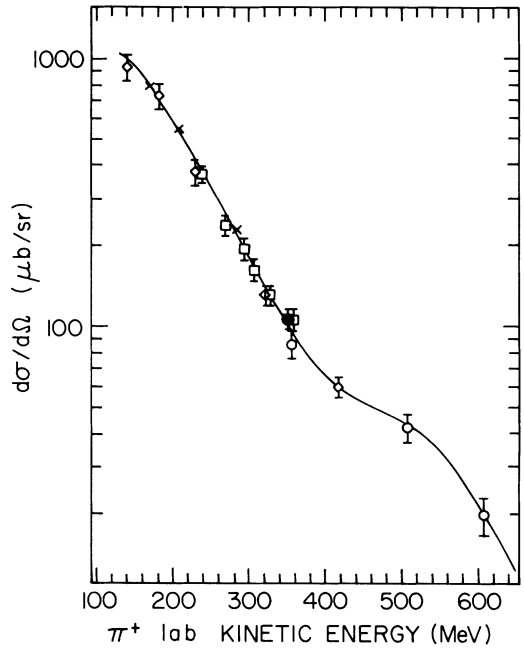

FIG. 4. Plot of $\pi^+ d \rightarrow pp$ differential cross section at 90° c.m. vs beam energy. Curve is a polynomial fit used for interpolation, χ^2 per degree of freedom is 0.88. The data plotted are diamonds, Boswell *et al.* (Ref. 25); crosses, Mathie *et al.* (Ref. 26); boxes, Mayer *et al.* (Ref. 27); closed circle, Chapman *et al.* (Ref. 28); and open circles, Heinz *et al.* (Ref. 29).

the arms were set to measure $\pi^+ d \rightarrow pp$ at 90° in the center of mass. The monitor scale factors were normalized to the known differential cross sections[25–29] (Fig. 4). We estimate the overall normalization uncertainty of these data to be about 15%. Secondly, we measured $\pi^+ d \rightarrow \pi^+ pn$ near the $\pi^+ p$ QFS peak, where the final state neutron lab momentum is zero. The data allowed precise determination of the spectrometer momentum calibration, alignment of the detectors, and verification of energy-loss calculations under the conditions used in the data analysis. The QFS angle pairs are listed in Table I. The QFS data are plotted in Fig. 5.

C. Momentum spectra

For every event which passed the coincidence condition, pulse heights, times, and positions were recorded on magnetic tape by a CAMAC microprogrammed input-output processor and a PDP 11/34 computer system. In the subsequent analysis, the trajectories of these events were required to originate in the target volume, pass between the magnet poles, and exhibit times of flight appropriate to the reaction kinematics. This reduced the accidental background to less than 1% for the vast majority of the data and less than 10% for all data. Accidental levels of 10%, caused by the 5-ns beam structure, occurred on two 425 MeV/c data sets, for $\theta_\Delta = 77°$ at $p_\pi = 270$ MeV/c and for $\theta_\Delta = 91°$ at $p_\pi = 290$ MeV/c, where they are responsible for the obvious anamolies in the data. Individual events were corrected for energy loss within the system. A lower cutoff at 40 MeV (280 MeV/c) was imposed on the proton energy to limit the energy-loss corrections. Efficiency and dead time corrections were made on a run by run basis.

For each momentum bin i, the measured cross section is given by

$$\left[\frac{d^3\sigma}{d\Omega_\pi d\Omega_p dp_\pi}\right]_i = \frac{(N_c)_i}{N_t N_b (\Delta\Omega_1 \Delta\Omega_2)_i \Delta p} . \quad (3)$$

The bin width Δp is 10 MeV/c. $(N_c)_i$ is the number of events in the bin, corrected for efficiency, dead time, and accidentals. N_t is the number of target particles per unit area, N_b is the integrated number of beam particles; the product $N_t N_b$ is measured by the calibrated beam monitors. The solid angle acceptance of the two arms, $(\Delta\Omega_1 \Delta\Omega_2)_i$, was determined for each bin by a Monte Carlo calculation which included pion decay and energy loss. The acceptance of the spectometer was at a maximum at 200 MeV/c and dropped below 30% above 350 MeV/c. Consequently the data above this pion momentum are less reliable and are not presented. The relative systematic error in the spectrometer acceptance is estimated to be about 5% when the acceptance has dropped to the 30% level due mainly to the uncertainty in $\Delta p/p$. This is small compared to the overall normalization uncertainty of 15%. Data taking was of sufficient length to accumulate at least 10–20 counts per μb/sr^2 in every 10 MeV/c bin at most energies and angle pairs. At angle pairs (θ_π, θ_p) containing large cross sections due to a strong QFS peak, this was proportionally reduced to as low as 2 counts per μb/sr^2/10 MeV/c (e.g., at $P_B = 350$ MeV/c, $\theta_\pi = 95$, $\theta_p = 25$).

The data at each angle pair are plotted in Figs. 6 and 7 versus the lab momentum (at the interaction point) of the measured pion. The small effect of averaging over the accepted angles and the 10 MeV/c momentum bins has been removed from the data by Monte Carlo simulation. The ratio between the theoretical cross section averaged over the acceptance of the apparatus and the theoretical cross section at the center of the bin in angles and momenta was used to correct the data. The correction was less than 10% in the regions of Δ^{++}, and as large as 30%

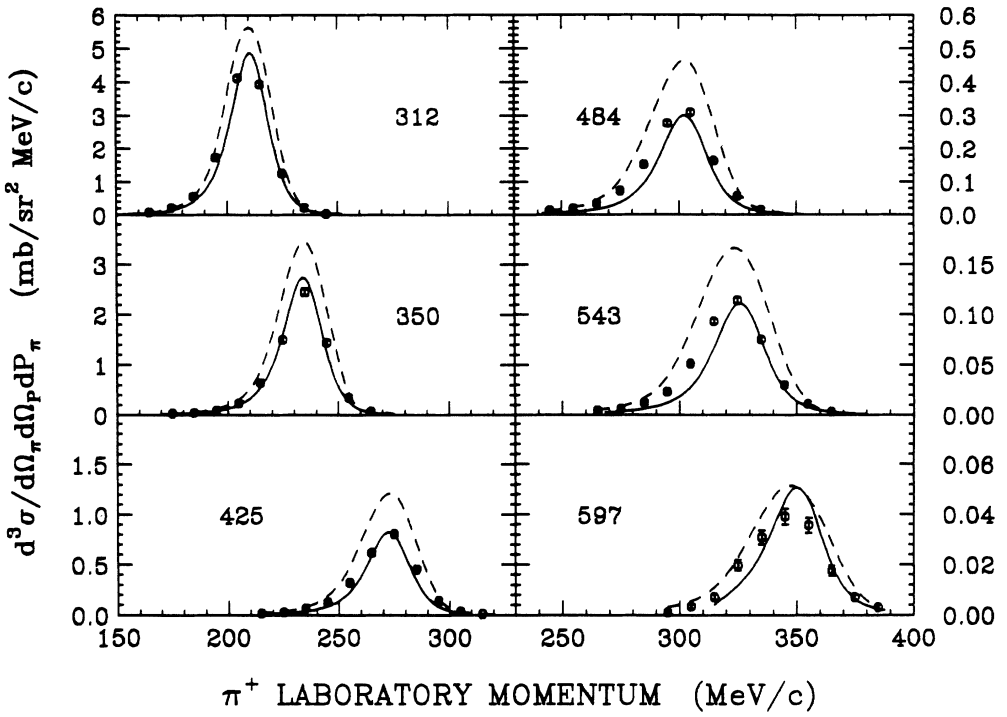

FIG. 5. Plot of $d^3\sigma/d\Omega_\pi d\Omega_p dp_\pi$ at QFS peak. Solid curve is due to Laget, dashed curve is due to Garcilazo.

at the QFS peak. The statistical accuracy of the correction is at most 3%. The systematic accuracy of the correction is harder to quantify. As long as the shape of the theoretical distribution reproduces the shape of the data in nearby regions of phase space, the correction will introduce little, if any, distortion in the deduced cross section. More details of the apparatus, analysis methods, and corrections may be found in Ref. 30.

Figures 6 and 7 show our data away from the zero neutron momentum kinematics, with the center of the Δ^{++} mass indicated in each case. Error bars indicate statistical errors only. A strong QFS peak is still obvious at many of the angle pairs, but becomes less prominent at angle pairs (θ_π, θ_p) with larger minimum spectator momentum. The minimum spectator momenta for events accepted by the apparatus are listed in Table I.

D. $\pi^+ d \to \Delta^{++} n$ cross sections

As was stated in the Introduction, the kinematics were chosen to emphasize the $n\Delta$ final state interaction. In order to concentrate exclusively on Δ production, additional kinematic cuts were made on the raw data. The events were binned in a two-dimensional histogram (Fig. 8) of Δ^{++} mass versus the center-of-mass scattering angle $\theta_{\Delta\text{c.m.}}$. Then only data with M_Δ between 1210 and 1260 MeV/c^2, and $\theta_{\Delta\text{c.m.}}$ in a ten-degree range about a given central value were accepted, as indicated by the dashed lines in Fig. 8. For each beam energy and detector angle pair, we calculated the following differential cross section:

$$\frac{d^3\sigma}{d\Omega_{\Delta\text{c.m.}} d\Omega_{\text{dec}} dM_\Delta} = \frac{N_c'}{N_l N_b (\Delta\Omega_{\Delta\text{c.m.}} \Delta\Omega_{\text{dec}}) \Delta M} \quad (4)$$

in microbarns per sr^2 MeV/c^2, where N_c' is the total number of events corrected for efficiency and dead time, which pass all previous cuts and the two-dimensional cut described above, as shown in Fig. 8. ΔM was taken to be 50 MeV/c^2 full width, rather than the width of the Δ^{++} to limit the effects of other diagrams, and to maintain a constant bin width at all beam energies. (The full Δ^{++} width was not available at $P_B = 312$ MeV/c.) $\Delta\Omega_{\Delta\text{c.m.}} \Delta\Omega_{\text{dec}}$ is the system solid angle product in Δ^{++} production and decay angles. This factor is calculated by a Monte Carlo simulation of the Δ production and decay process in the experimental apparatus, with the same cuts on M_Δ and $\theta_{\Delta\text{c.m.}}$ as were applied to the corresponding data set.

Insofar as the pion interacts almost exclusively with the proton via the resonant P_{33} partial wave, the choice of kinematics dictates that this is the $\pi^+ d \to n\Delta^{++}$ cross section. This point is discussed further in Sec. III, where it will be seen that the Δ^{++} provides at least 90% of the cross section. Thus the procedure described above gives the $\pi^+ d \to n\Delta^{++}$ cross section in terms of the Δ^{++} production angle in the reaction center-of-mass frame, and the decay angle of the proton θ_{dec} with respect to the Δ^{++} c.m. velocity vector, in the Δ^{++} rest frame. This latter angle is always between 15° and 35°. The data were corrected for finite bin width in a manner similar to the one described in Sec. II C. The differential cross sections are compiled in Table II, along with the correction fac-

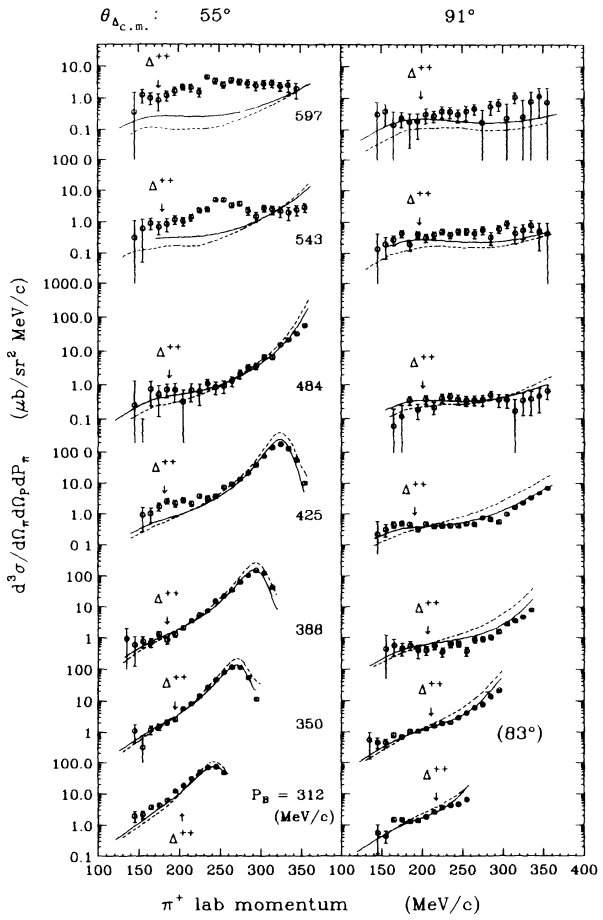

FIG. 6. Plots of $d^3\sigma/d\Omega_\pi d\Omega_p dp_\pi$ vs pion momentum for Δ production angles $\theta_{\Delta c.m.}$ of 55° and 91°, except where indicated otherwise. Error bars are statistical only. Solid curve is the multiple scattering calculation of Laget, and the dashed curve is the Faddeev calculation of Garcilazo. Associated detector and decay angles may be found in Table I. Center of Δ^{++} mass distribution is marked with an arrow in each case.

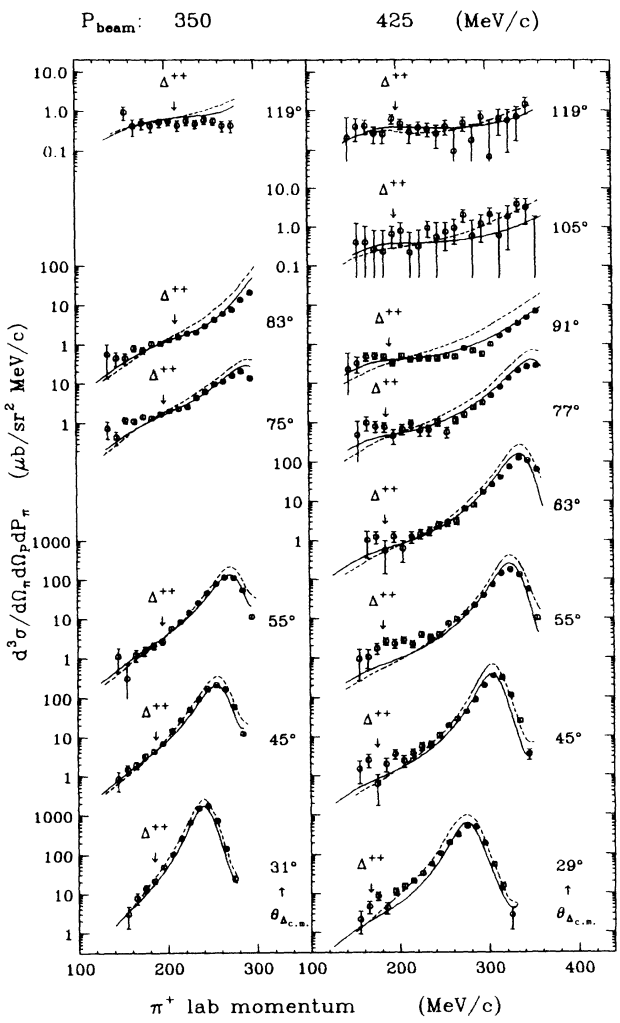

FIG. 7. Plots of $d^3\sigma/d\Omega_\pi d\Omega_p dp_\pi$ vs pion momentum at 350 and 425 MeV/c beam momenta, see Fig. 6 caption.

tors used. In Figs. 9 and 10, these results are plotted against $\theta_{\Delta c.m.}$ and the beam momentum.

III. THEORY

As stated in the Introduction, there are two different types of theories available, the multiple scattering or diagrammatic approach, and the relativistic Faddeev calculation. We will compare the data to two such theories, the Faddeev calculations of Garcilazo[17–20] and the multiple scattering calculations of Laget.[31]

A. Faddeev theory

The pion-induced deuteron breakup, under suitable approximations, can be reduced to a Faddeev theory with only pairwise interactions between the three particles. Theories based on the formalism of Aaron, Amado, and Young[32] (AAY) have had some success in describing nucleon-nucleon scattering as well as πd elastic scattering (see Ref. 23 and references therein). The Faddeev theory satisfies three-body unitarity, so it can be applied to πd inelastic channels as well. Garcilazo solves the isobar or separable approximation for the relativistic two-particle T matrices numerically using Padé approximants. The T matrices are constructed directly from experimental phase shifts for the πN subsystem, and from an analytic approximation to the Paris potential[33] for the NN subsystem. Only the six S and P wave πN partial waves and the two S wave NN partial waves are included. This latter approximation takes explicit account of the $^3S_1$-$^3D_1$ bound state and the $^1S_0$ antibound state poles in the NN amplitude, which dominate the FSI region of phase space. There are no free parameters. No exotic particles or unusual diagrams are included. Three-particle unitarity is obeyed, but no diagrams with more than three particles in an intermediate state are explicitly included. The Δ^{++} isobar is incorporated via the P_{33} resonant partial wave, but no explicit interactions between the Δ^{++} and the spectator neutron are considered. The full numerical

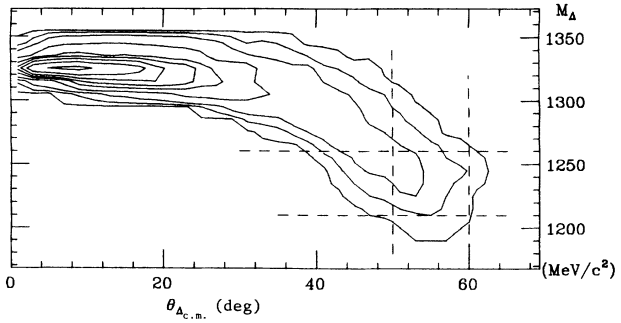

FIG. 8. Contour plot showing the distribution of events for the data set taken at $\theta_\pi = 70°$, $\theta_p = 50°$, $P_B = 425$ MeV/c plotted against Δ^{++} mass M_Δ and production angle $\theta_{\Delta c.m.}$. Dashed cuts are used to calculate cross sections of Table II plotted in Figs. 10 and 11. The outermost contour corresponds to two events per 2° by 10 MeV/c bin and each successive contour is a factor of 2 larger.

solution was performed for values of the total angular momentum J up to 5, thereafter the impulse approximation was used for J up to 14.

Figure 11 shows some sample results of the theory. In each case the solid curve is the full calculation, the dotted curve has the resonant P_{33} πN partial wave amplitude deleted, and the dashed curve includes only the P_{33} partial wave. The basic features of the impulse approximation can still be seen. The peak on the right of each plot occurs where the neutron laboratory momentum passes through a minimum value, indicating that the deuteron wave function dominates the shape as a function of the spectator momentum. The pion interacts almost exclusively with the proton in the deuteron via the resonant P_{33} partial wave, and provides as much as 90% of the cross section at the position of the Δ^{++} peak. Interference from nonresonant partial waves is a small effect, as shown by the small difference between the dashed and solid curves. This extreme dependence on the Δ^{++} is of course partially due to the choice of kinematics. Because of the large width of the Δ^{++} (115 MeV/c^2) the enhancement of the cross section is only visible when it is outside the region of the strong momentum dependence near the QFS peak [Figs. 12(c) and 12(d)]. The cross section minima below 100 MeV/c pion momentum corresponds to the maximum proton momentum.

B. Multiple scattering theory

Laget has calculated pion-induced deuteron breakup using a multiple scattering formalism. The amplitude includes the coherent sum of the pole or QFS diagram, Fig.

TABLE II. $\pi^+ d \to \Delta^{++} n$ cross sections. Corresponding to each entry in Table I, there is a threefold differential cross section in the Δ mass, production, and decay angles. The results of the analysis of Sec. II D are shown with statistical errors. The momentum of the spectator nucleon is also given in the laboratory frame of reference. The factor listed in the last column is the solid angle correction factor (see text). These data are plotted in Figs. 9 and 10.

Beam momentum (MeV/c)	$\theta_{\Delta c.m.}$	$\frac{d^3\sigma}{d\Omega_{\Delta c.m.} d\Omega_{dec} dM_\Delta}$ $\left[\frac{\mu b}{sr^2 MeV/c^2}\right]$ p_n (MeV/c)	Data	Factor
311.6	55°	137.1	4.59 ±0.22	1.15
	91°	210.4	0.699±0.039	1.08
	31°	136.3	6.44 ±0.21	0.823
	45°	171.5	2.72 ±0.18	0.835
350.3	55°	197.8	1.85 ±0.15	0.876
	75°	249.3	0.965±0.059	1.00
	83°	268.9	0.756±0.056	1.01
	119°	343.2	0.386±0.050	0.994
387.6	55°	246.1	0.529±0.061	0.936
	91°	347.6	0.252±0.035	1.01
	29°	211.2	1.78 ±0.36	0.901
	45°	256.4	0.748±0.188	0.940
	55°	287.8	0.765±0.097	0.964
425.0	63°	313.4	0.405±0.084	0.983
	77°	357.8	0.389±0.054	0.992
	91°	400.1	0.337±0.030	1.00
	105°	438.8	0.312±0.071	0.988
	119°	472.6	0.354±0.053	1.00
483.8	55°	343.9	0.421±0.091	0.977
	91°	472.9	0.259±0.042	1.03
543.0	55°	392.9	0.568±0.099	1.05
	91°	538.5	0.234±0.035	1.02
597.0	55°	432.9	0.824±0.140	1.00
	89°	584.8	0.185±0.038	1.03

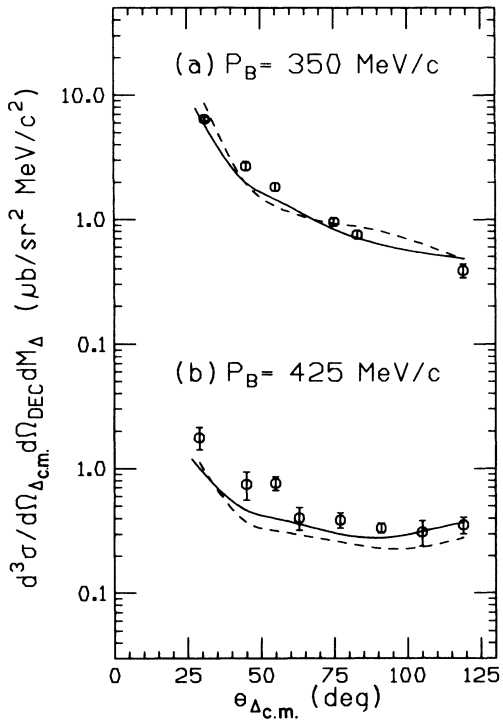

FIG. 9. $\pi^+ d \to \Delta^{++} n$ angular distributions at 350 and 425 MeV/c, statistical errors only. The solid curve is the multiple scattering calculation of Laget, the dashed curve is the Faddeev calculation of Garcilazo.

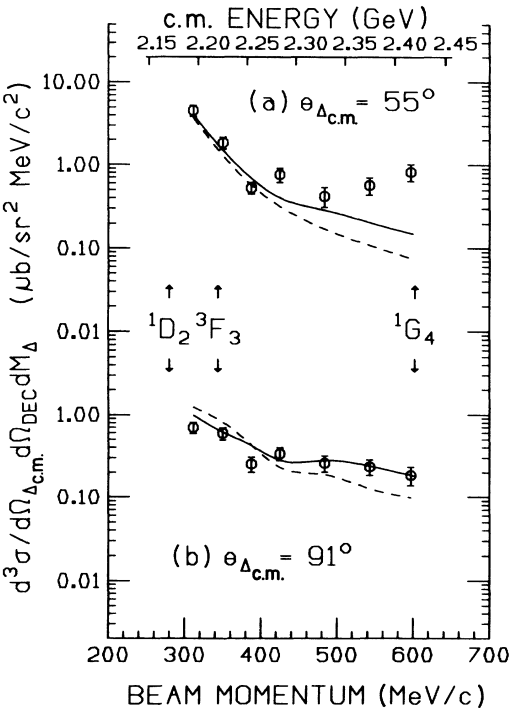

FIG. 10. $\pi^+ d \to \Delta^{++} n$ differential cross section as a function of the beam momentum at 55° and 91° c.m. The curves are explained in Fig. 9. The point at 350 MeV/c in (b) is interpolated from Fig. 9(a). Top scale is total center of mass energy in GeV. Locations of proposed dibaryons in the pp system are marked with vertical arrows. Errors include statistical errors added in quadrature to the 15% normalization errors.

1(a), πN rescattering diagrams, Fig. 1(b), NN rescattering diagrams, Fig. 1(c), and πN double scattering diagrams, Fig. 1(d). The Reid[34] deuteron wave function was used. The P_{33} wave part of the πN subsystem was parametrized as the Δ^{++} resonance using a nonrelativistic reduction, of order $1/M_p^2$, while the other partial waves are parametrized by πN phase shifts. Since the scattered pion in Fig. 1(b) or 1(d) can be far off shell, the pion-baryon vertex was parametrized by a monopole form factor,

$$F_\pi(q^2)=\frac{\Lambda_\pi^2-m_\pi^2}{\Lambda_\pi^2-q_\pi^2}\ , \tag{5}$$

where q_π^2 is the virtual mass squared of the pion and

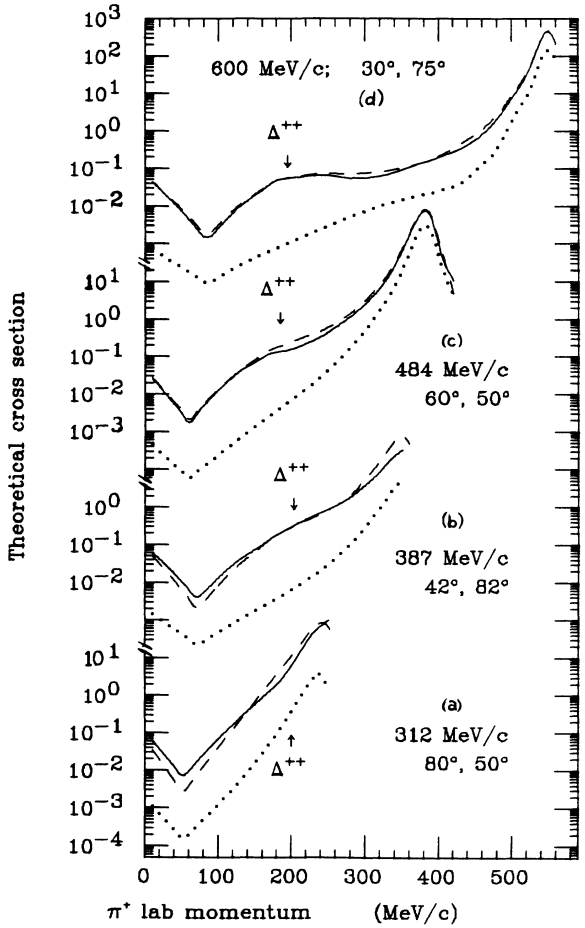

FIG. 11. Comparisons of the full Faddeev prediction with predictions for two partial calculations. The comparison is made for four angle pairs from the present data set, in order of increasing beam energy. The solid curve in each case is the full prediction. For the dotted curve, the resonant P_{33} partial wave contribution was removed from the calculation. The dashed curve is the result of the calculation including only the P_{33} partial wave in the πp interaction. A vertical arrow marks the center of the Δ mass distribution in each case.

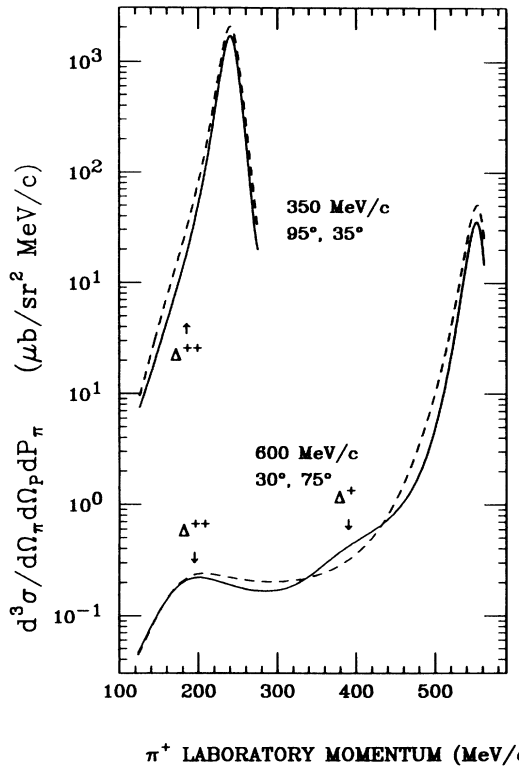

FIG. 12. Multiple scattering calculation of the $\pi^+ d \to \pi^+ pn$ reaction. The dashed curve is the QFS diagram Fig. 1(a) with only the $\pi^+ p$ interaction. The solid curve contains a coherent sum of diagrams 1(a)–1(d) with both $\pi^+ p$ and $\pi^+ n$ interactions at the πN vertex.

$\Lambda_\pi = 1.2$ GeV is the cutoff mass. The nucleon-nucleon rescattering amplitude in diagram 1(c) was factorized out of the integral. This is correct for S waves but not for P waves. Higher-order effects, such as $N\Delta$ [Figs. 1(e) and 1(f)] interactions or dibaryons, have not been included. The present data were not used to adjust any of these parameters. The calculation is a straightforward extension of the calculation of the $\gamma d \to pp\pi^-$ reaction cross section[31] where the elementary interaction $\gamma N \to N\pi$ has been replaced by the $\pi N \to \pi N$ amplitude. These calculations lead to fair agreement with the $\gamma d \to pp\pi^-$ kinematically complete and inclusive cross sections, especially near the QFS peak. In addition, the model has been applied to $\pi d \to pX$ inclusive measurements in the Δ resonance energy range, with more modest success.[35]

Figure 12 shows the contribution of the QFS graph, and the effect of including single and double scattering graphs. As was noted earlier, the addition of the rescattering terms reduces the QFS cross section by about 25% [Fig. 12(a)]. At higher energies, the various mechanisms become separated and easier to identify. In Fig. 12(b) the QFS, Δ^{++}, and Δ^+ terms can be clearly seen. In all cases, the product of the deuteron wave function and the πN P_{33} amplitude provides the scale of the cross section in the kinematic region of the present experiment.

IV. COMPARISON WITH DATA AND CONCLUSIONS

The above theories are compared with the present data in Figs. 5, 6, and 7. The multiple scattering theory of Laget is shown as a solid line. At the QFS peak the ratio of the theory to the data averages 1.00 ± 0.15, which is within the data normalization errors. The best agreement is found with the 350 MeV/c data. The 425 MeV/c data lies above the theory in the region of the Δ^{++} for forward θ_Δ. As a function of beam energy, the theory fits the 55° and 91° data well below 543 MeV/c. This is no longer true at the two highest energies, where the data have a P_n range of 150–600 MeV/c, with the Δ^{++} near 500 MeV/c. At such large momentum transfers, the deuteron wave functions used may not be valid and higher-order diagrams should begin to play a role.

The Garcilazo Faddeev calculation is shown as the dashed line. At the QFS peak, Fig. 5, the theory averages a factor of 1.43 larger than the data. This results in substantially worse agreement with the data below $P_n = 100$ MeV/c, than found in the Laget calculations. The reason for the 40% disagreement between the two theories at $P_n = 0$ MeV/c is not known. For $\theta_\Delta = 55°$, the Garcilazo result crosses the Laget result when $P_n = 150$ MeV/c for $P_B = 312$ MeV/c and at $P_n = 250$ MeV/c for $P_B = 485$ MeV/c. Similarly, the two results are equal at $P_n = 200$ MeV/c for $P_B = 312$ MeV/c and $P_n = 400$ MeV/c at $P_B = 485$ MeV/c when $\theta_\Delta = 90°$. The spectator momentum of the crossover point begins decreasing above this beam momentum. Since the crossover momentum usually is near the peak of the Δ^{++}, the two theories are generally in good agreement in this region.

As explained in Sec. II D, each point on Figs. 9 and 10 represents data from one angle pair, for a Δ^{++} mass range of 1210–1260 MeV/c^2 and a θ_Δ range of $\pm 5°$. These points correspond to the decay angles given in Table I. The data have been corrected for the average over the phase-space acceptance. The error bars in Fig. 9 are statistical only, while those in Fig. 10 include both the statistical error from Table II and the 15% normalization error added in quadrature. The two theories, evaluated at the center of the mass and angular bins, are also plotted. As can be seen in Fig. 9, the data and theories are in excellent agreement for the 350 MeV/c angular distribution. The Laget calculation lies generally above the Garcilazo calculation for the 425 MeV/c angular distribution, and both are below the data at angles forward of 90°. The energy dependence is shown in Fig. 10. The Laget calculation reproduces the 90° data at all energies, and the low-energy 55° data. The Garcilazo calculation falls approximately a factor of 2 below the Laget results above 425 MeV/c, with the data exceeding the theory by an order of magnitude at 600 MeV/c. The biggest discrepancies occur for $\theta_\Delta = 55°$ at 425 MeV/c and above. Higher partial waves beyond the S and P waves already included as input are not expected to make a significant contribution. Our choice of kinematics should make the small number of πN and NN partial waves a reasonable approximation, especially near the Δ^{++} mass peak. This is clear evidence that higher-order diagrams are becoming important. However, since the range of validity of

the two models has been exceeded, no definite conclusions about the need for exotic effects can be drawn. The apparent narrow dip at 387 MeV/c may be an artifact of either a normalization or momentum calibration error. A QFS run was not successfully taken at this energy; hence these quantities could not be double checked.

The most interesting possible explanations for the discrepancies are dynamic effects which are not included in the present calculations. Among the many specific possibilities, we mention two.

The first is a ΔN interaction [Figs. 1(e) and 1(f)]. Indeed, part of the ΔN interaction is already included in the Faddeev iteration $N\pi N \rightarrow N(\Delta) \rightarrow N\pi N \rightarrow (\Delta)N$ of Fig. 13(a). It can be variously described as two one-pion exchange (OPE) $N\Delta \rightarrow N\Delta$ amplitudes or a single two-pion exchange direct $N\Delta \rightarrow N\Delta$ amplitude. The diagram is included at some level in the multiple scattering diagram 1(f). The OPE direct amplitude illustrated in Fig. 13(b) is *not* included in either theory. Diagrams like this are beyond the three-particle limitations of the Faddeev theory, because the Δ is not treated as a particle on equal footing with the nucleons and pions. This amplitude can contribute to πd breakup as a Δn final state interaction, as shown in Fig. 13(c). Suppose that all of the final state momentum is transferred to the spectator nucleon in the last pion exchange [13(c)]. A simple estimate of the cross-section ratios at the Δ peak in the OPE model would give

$$\frac{\sigma(\theta_{\Delta\text{c.m.}}=55°)}{\sigma(\theta_{\Delta\text{c.m.}}=91°)}=\frac{(q^2+m_\pi^2)^2_{\theta_{\Delta\text{c.m.}}=91°}}{(q^2+m_\pi^2)^2_{\theta_{\Delta\text{c.m.}}=55°}}\ , \tag{6}$$

where q^2, the square of the four momentum transferred by the pion, is $2M_nT_n$, and T_n is the lab kinetic energy of the final state neutron. Over the three highest beam energies (Table II, Fig. 10), the ratio of the propagators squared is about 3, and the ratio of the experimental cross sections increases from about 2 up to 4. Without this Δn OPE term, the two theories predict a ratio of ~ 0.9. Of course, a detailed calculation of the one-pion exchange model is necessary at the large momentum transfers ($q_\pi \simeq 4m_\pi$) required by the kinematics. We have also made estimates of the amplitude of Fig. 1(e) with a resonant Δn interaction and a virtual on-resonance Δ. A ΔN resonance energy about 90 MeV above the ΔN threshold is required to enhance the cross section by an order of magnitude. However, no attempt has been made to include a specific dibaryon resonance or ΔN interaction. More theoretical work is required before these data can make a more definite statement about the specific ΔN interaction involved.

Another possibility which goes beyond the limitations of present calculations is a genuine three-body force by which the incident pion interacts with the whole deuteron instead of just one of the constituents [Fig. 13(d)]. The interesting feature of this amplitude is that both nucleons are excited to Δ's, each with nearly half the pion energy and momentum. Both Δ's can be near resonance and the nucleons in the deuteron at nearly zero relative momentum simultaneously, thereby making a large contribution to the cross section. Again, only a complete calculation can decide the importance of such a process.

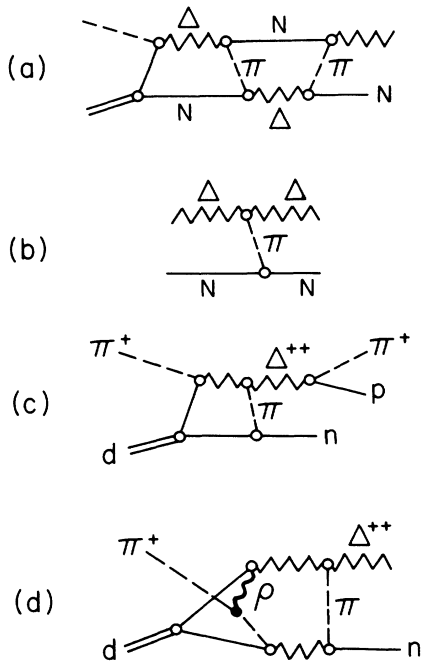

FIG. 13. (a) Faddeev iteration in πN P_{33} partial waves, constituting part of a ΔN interaction. (b) Direct single-pion exchange between the Δ and a nucleon, not included in the theory. (c) (b) included in a πd breakup diagram as a Δn FSI, part of Fig. 1(e). (d) Possible three-body force contribution to πd breakup.

In conclusion, by a suitable choice of kinematics we have succeeded in isolating regions of phase space where the $\pi^+ d \rightarrow \pi^+ pn$ breakup is dominated by the $\pi^+ d \rightarrow \Delta^{++} n$ reaction. The two theories reproduce the data quite well except at 55° at the highest energies. The indications are that some process is at work which is not treated in the present theory. Such a process is required to give the spectator neutron a large momentum (compared to its Fermi momentum) with much greater probability than the processes which are presently well understood. A direct interaction between the Δ and the neutron may be able to supply the required momentum.

ACKNOWLEDGMENTS

The authors would like to acknowledge the help of many persons on the staff of the Los Alamos Meson Physics Facility, especially Peter Gram, Dan Fitzgerald, and Bob Damjanovich. We are also indebted to Paul Stoler and collaborators for contributing the method of isolating the $n\Delta$ pair by kinematic restrictions. Finally, we would like to thank William Turchinetz for suggesting this problem. This work was supported by the U.S. Department of Energy on DE-FG05-87ER40309.

*Present address: Indiana University Cyclotron Facility, Bloomington, IN 47405.
†On leave from Escuela Superior de Fisica y Matematicas, Instituto Politecnico Nacional, México 14 D.F., México.

[1]T. E. O. Ericson, CERN-TH Report No. 4994/88, 1988.
[2]M. Araki, Y. Koike, and T. Ueda, Prog. Theor. Phys. **63**, 2133 (1980).
[3]I. Duck and E. Umland, Phys. Lett. **96B**, 230 (1980).
[4]W. Grein, K. Kubodera, and M. P. Locher, Nucl. Phys. **A356**, 269 (1981).
[5]Yu. D. Bayukov *et al.*, Yad. Fiz. **20**, 59 (1974) [Sov. J. Nucl. Phys. **20**, 30 (1975)].
[6]Yu. D. Bayukov *et al.*, Nucl. Phys. **A282**, 389 (1977).
[7]L. G. Dakhno *et al.*, Pis'ma Zh. Eksp. Teor. Fiz. **30**, 467 (1979) [JETP Lett. **30**, 436 (1979)].
[8]L. G. Dakhno *et al.*, Yad. Fiz. **31**, 630 (1980) [Sov. J. Nucl. Phys. **31**, 328 (1980)].
[9]L. G. Dakhno *et al.*, Pis'ma Zh. Eksp. Teor. Fiz. **34**, 296 (1981) [JETP Lett. **34**, 283 (1981)].
[10]L. G. Dakhno *et al.*, Phys. Lett. **123B**, 33 (1983).
[11]L. G. Dakhno *et al.*, Nucl. Phys. **A414**, 477 (1984).
[12]G. Z. Obrant, Yad. Fiz. **36**, 862 (1982) [Sov. J. Nucl. Phys. **36**, 504 (1982)].
[13]J. H. Hoftiezer *et al.*, Phys. Lett. **88B**, 73 (1979).
[14]J. H. Hoftiezer *et al.*, Phys. Rev. C **23**, 407 (1981).
[15]M. M. Makarov, G. Z. Obrant, and V. V. Sarantsev, Phys. Lett. **122B**, 343 (1983).
[16]A. Matsuyama, Nucl. Phys. **A379**, 415 (1982).
[17]H. Garcilazo, Phys. Rev. Lett. **48**, 577 (1982).
[18]F. Goetz *et al.*, Phys. Rev. C **31**, 1563 (1985).
[19]W. Gyles *et al.*, Phys. Rev. C **33**, 583 (1986); **33**, 595 (1986).
[20]H. Garcilazo, Phys. Rev. Lett. **45**, 780 (1980); Nucl. Phys. **A369**, 411 (1981); Phys. Rev. Lett. **53**, 652 (1984).
[21]The calculations presented in Ref. 19 are in error. They must be multiplied by a factor of 2. See also Ref. 22, p. 1588.
[22]W. List *et al.*, Phys. Rev. C **37**, 1587 (1988); **37**, 1594 (1988).
[23]H. Garcilazo, Phys. Rev. C **35**, 1804 (1987).
[24]E. Colton, Nucl. Instrum. Methods **178**, 95 (1980).
[25]J. Boswell *et al.*, Phys. Rev. C **25**, 2540 (1982).
[26]E. L. Mathie *et al.*, Z. Phys. A **313**, 105 (1983).
[27]B. Mayer *et al.*, Nucl. Phys. **A437**, 630 (1985).
[28]K. R. Chapman *et al.*, Phys. Lett. **11**, 253 (1964).
[29]R. M. Heinz, O. E. Overseth, D. E. Pellett, M. L. Perl, Phys. Rev. **167**, 1232 (1968).
[30]P. V. Pancella, Ph.D. thesis, Rice University, 1987.
[31]J. M. Laget, Phys. Rep. **69**, 1 (1981).
[32]R. Aaron, R. D. Amado, and J. E. Young, Phys. Rev. **174**, 2022 (1968).
[33]M. Lacombe *et al.*, Phys. Rev. C **21**, 861 (1980); Phys. Lett. **101B**, 139 (1981).
[34]R. V. Reid, Ann. Phys. (N.Y.) **50**, 419 (1968).
[35]J. Arvieux *et al.*, Nucl. Phys. **A444**, 579 (1985).